Proceedings of the
Annual Stability Conference
Structural Stability Research Council
Charlotte, North Carolina, April 11-14, 2023

Design of steel beams affected by local/global coupled instabilities

Lucile Gérard[1], Nicolas Boissonnade[2]

Abstract

The present paper investigates the resistance of I and H-shapes subjected to uniform major-axis bending moment and prone to suffer from local/global coupling effects. Numerical parametric studies allowed the determination of local/global coupling functions for hot-rolled and welded sections aiming at correcting the influence of local effects – which tends to decrease – when the member slenderness increases. These functions, included into an O.I.C.-type design approach, may be seen as an alternative to the current Eurocode rules in which local/global interactions are roughly accounted for through the global relative slenderness definition and a rather conservative final strength verification. A formulation predicting the strength of beams made of such sections is then eventually suggested. These design proposals were seen to lead to great improvements in accuracy and consistency compared to current European provisions.

1. Introduction

The present paper aims at investigating the member response of unrestrained beams made of slender I and H-shapes to provide design formulations leading to a precise estimation of beams ultimate capacities obtained numerically – based on a F.E. model validated against test series.

Towards an increased use of thin-walled sections made of high strength steel whose local capacity is mostly governed by local buckling, the design of steel beams made of slender I and H-sections – thus prone to suffer from coupled Lateral Torsional Buckling (L.T.B.) and local buckling – represents a strategic challenge. A precise prediction of their strength shall allow for important material savings compared to what is currently achieved by means of code provisions.

In that context, a proper assessment of the variation in local buckling influence together with the member slenderness represents a key aspect: typically not considered in present codes directives, it may allow for lighter and safer structures resulting into easier handlings throughout the construction. Indeed, members may be allowed to carry higher strengths once they are no longer penalised by a high local buckling influence.

Needs for improved design rules arise from the many insufficiencies actually provided in codes. As an example, the Eurocode design directives (EN 1993-1-1 2005) for beams prone to

[1] PhD, Laval University, <lucile.gerard.1@ulaval.ca>
[2] Professor, Laval University, <nicolas.boissonnade@gci.ulaval.ca>

experience L.T.B. can be shown to exhibit some important shortcomings which may be listed as follows:

- The dependency of L.T.B. curves on the height-to-width ratio as unique key parameter shall be questioned and recent developments from Taras (Taras 2011) emphasize that beams capacities shall be sorted using a more precise parameter to provide reliable strength prediction;
- The reach of strengths higher than the elastic critical buckling bending moment highlighted by Taras (Taras 2011) is not accounted for in current provisions;
- Elements prone to suffer from high local/global coupling are still not efficiently designed in current codes design rules. Indeed, while the introduction of local buckling into the definition of the global LTB relative slenderness allows reaching higher global reduction factors, the full reduction owing to local buckling is still in effect on the final strength check suggested in the Eurocode. Such verification is over-conservative since slender members mostly fail owing to global buckling.

In that context, several researchers focused on the development of design proposals able to provide alternatives and improvements to what is currently suggested in codes. Towards its aim to address the design of beam-columns, Villette (Villette 2003-2004) suggested strength curves equations for beams under pure major-axis bending through both the Merchant-Rankine formulation and Ayrton-Perry format. Villette also proposed design rules for welded sections with flame-cut flanges.

One of Villette's design proposals includes the effects of pre-buckling deflections by means of a correction factor $(1 - I_z / I_y)^{0.5}$ applied to the elastic critical bending moment M_{cr} which is involved in the global relative slenderness. Further to this aspect, Villette's proposal relies on the influence of the ratio $h^2 \cdot t_w / (b^2 \cdot t_f)$.

Several years later and consecutively to deep numerical series on open-sections under major-axis bending, Taras (Taras 2011) (Taras et Greiner 2010) suggested another design proposal whose ultimate purpose is to replace the one currently used in Europe.

An important aspect which deserves to be noticed about the Eurocode's design curves for L.T.B is the use of an Ayrton-Perry formulation which is primarily suited to flexural buckling mechanical behaviour. Accordingly, Taras, with the help of developments arising from previous studies, first adapted the buckling curves formulation to fit mechanically to an element suffering from L.T.B. As addressed by Ayrton-Perry for flexural buckling, the development is based on 2nd order equilibrium with initial geometrical imperfections and relies on an elastic failure criterion. Although the formulation does not include the effects of plasticity, the author noticed it would not change drastically the accuracy but still it may significantly raise the design complexity. Taras' proposal relies on the height-to-width ratio and section yield moduli. h / b ratio allows for a first separation between beams and columns shapes which is then refined through ratio $(W_{y,el} / W_{z,el})^{0.5}$. Such formulation enables to account for (i) the higher influence of residual stresses on column shapes which has been stated for many years and is coherent with the residual stresses pattern used by the author in his numerical series, and (ii) the increased strength typically highlighted by column shapes against lateral torsional buckling due to their higher weak-axis stiffness and lower $(W_{y,el} / W_{z,el})^{0.5}$ ratios, resulting in lower imperfection factors, sources of more favourable strength curves. Taras design proposal leads to greater strength predictions for hot-rolled compact to semi-compact sections than the current L.T.B. curves suggested by the Eurocode, thanks to a higher accuracy provided by the new parameters proposed. However, several comments may be pointed out:

- As specified by Taras in his thesis (Taras 2011), this proposal provides less reliable strength predictions for unconventional geometries (typically produced by welding);
- Strengths higher than the elastic critical bending moment were not accounted for in the design although such resistances were observed by the author for slender beams;
- Local and global behaviours are not distinguished, so that when local buckling becomes determinant for slender sections (not considered in Taras study which was restrained to Class 1, 2 and 3), the design may not provide an accurate prediction of their strength and local/global interactions are not addressed;
- In addition, since the author did not isolate local behaviour from global behaviour, it may not be possible to implement the design as it is into the O.I.C.

Both proposals described above did not include any consideration of local/global coupling behaviours mostly expected at intermediate slenderness of members made of slender sections.

Few studies have been achieved on the subject but the work from Hayeck (Hayeck 2016), Couto *et al.* (Couto, Vila Real et Lopes, et al. 2016) (Couto et Vila Real April 2-5, 2019), and Schillo *et al.* (Schillo et Feldmann November 7-8 2016) shall be noticed to better apprehend how coupling effects may be considered in the O.I.C. approach.

Schillo *et al.* (Schillo et Feldmann November 7-8 2016) conducted experimental tests to investigate the interaction between local and global buckling of box sections under axial force. The authors suggested a modification to the usual form of the "equivalent imperfection" η used in the Ayrton-Perry formulation to account for local effects. While the initial form was $\eta = e_0 \cdot A / W$, Schillo *et al.* suggested $\eta = (e_0 + e_p) \cdot A / W$ where $e_p = \max(0;136.4^3 \lambda_p^2 - 254.3\lambda_p + 112)$. This equation which depends on a unique λ_p may be appropriate only for quadratic box section presenting unique plate slenderness with similar boundary conditions. An expression for the global reduction factor χ_c was then derived which accounts for the local strength through e_p, local, global and coupled local/global elastic critical buckling behaviours by means of the relative slenderness definition of λ_{GM}. In such proposal, the influence of plasticity on the local/global interactions is not explicitly accounted for.

More recently, Hayeck studied the influence of a section high slenderness in a column global capacity (see (Hayeck 2016) and (Li, et al. 2017)). Extensive numerical series were carried out on highly slender sections so as to understand how this influence shall be included into her initial O.I.C. proposal for members under axial force only. The author highlighted the great difference between the maximum stress at the section suffering from the highest second-order effects compared to the average stress present on the member. It raised some doubts on whether the full section capacity or an effective one shall be used to approach the mechanical behaviour more closely.

Quite recently too, Couto *et al.* (Couto, Vila Real et Lopes, et al. 2016) studied the behaviour of slender I-shapes subject to Lateral Torsional Buckling under fire conditions. The authors conducted extensive numerical investigations and suggested a design proposal based on the ratio of the effective section yield modulus over the full section yield modulus $s = W_{eff,y} / W_{el,y}$, however not continuous between doubly-symmetric sections geometries. Subsequently, Couto *et al.* suggested a design equation which mostly follows the current rules in the Eurocode using Ayrton-Perry formulation. As a result of observations on the local/global interaction for several

[3] λ_p represents the plate relative slenderness and is determined according to the Eurocode directives.

values of ratio s, the authors suggested the values reported in Table 1 for the imperfection factor α_{LT} – note that α_{LT} definitions account for the material yield strength.

Table 1: Definition of the imperfection factor α_{LT} suggested by Couto *et al.* (Couto, Vila Real et Lopes, et al. 2016).

Slenderness among Class 4 sections	Limits of s	α_{LT}	$\lambda_{LT,0}$
Low	$s > 0.9$	$1.25 \cdot (235 / F_y)^{0.5}$	0.2
Intermediate	$0.9 > s > 0.8$	$1.00 \cdot (235 / F_y)^{0.5}$	0.2
High	$s \leq 0.8$	$0.75 \cdot (235 / F_y)^{0.5}$	0.2

While many efforts were put into the determination of design proposals predicting beams strengths, only few studies did focus on slender sections. Indeed, Taras highlighted that his formulation may not be valid for sections shapes far from conventional geometries – typically suffering from high local effects. As for researchers who investigated the ultimate capacity of members suffering from coupled local and global buckling, Hayeck only focused on hollow shapes and Couto's proposal although suitable for I and H-shapes is not continuous between doubly-symmetric sections geometries.

Through a straightforward approach such as the O.I.C. (Boissonnade, et al. 2017), beams strengths can be predicted directly through a design method explicitly expressing beams and columns mechanical behaviours. Assessing and quantifying local/global coupling effects for several member slenderness would allow for such design to rely on a more precise mechanical background. Applications would benefit from a more accurate consideration of local buckling influence together with the member slenderness through the acknowledgment of beams made of slender sections to reach higher strengths at high global slenderness. However, such case has neither been addressed completely through previous investigations nor been dealt with yet within the development of the O.I.C.

Towards the development of a design proposal directly predicting the strength of beams made of compact to very slender sections, for hot-rolled and welded manufacturing processes, continuous between doubly-symmetric sections geometries and allowing for an explicit assessment of local/global interactions, numerical parametric studies were carried out on many sections shapes using a F.E. model whose reliability was first carefully assessed. A brief sub-study was carried out to determine reliable amplitudes to apply to geometrical and material imperfections to guarantee the obtainment of reliable ultimate capacities. Numerical studies on several members with different yield stresses, lengths and sections shapes allowed the determination of design curves after a careful investigation on the extent of local buckling influence with the member slenderness.

In the present paper, the F.E. model general features will be first described in section 0. This section also reports the assessment of the F.E. model reliability through comparisons against test series, as well as a brief investigation on the influence of imperfections on beams strength so that reasonable amplitudes can be eventually adopted. Then, parametric studies on the member strength of hot-rolled and welded sections possibly suffering from local buckling are detailed in section 0. A design proposal for hot-rolled sections is then suggested. Conclusions are highlighted through section 0.

2. Finite Element model

2.1 General features

FINELg software was used for the entire investigation (Liège University, Greisch ingénierie 2005). The software has been used successfully in many applications and its reliability has been assessed in several verifications of F.E. models accuracy through comparisons with tests data. The works of Nseir (Nseir 2015), Hayeck (Hayeck 2016) and Gérard (Gérard 2020) may be noticed among others.

G.M.N.I.A. and L.B.A. analyses were performed using a F.E. model based on four nodes shell elements. Both hot-rolled and welded I and H-sections were tested and some additional truss and beam elements were introduced uniquely for hot-rolled sections to appropriately account for the internal radius stiffness.

Loading was applied by means of axial forces on the four flanges tips except for the comparison with experimental data in which the experimental set-up was modelled as precisely as possible. Fork support conditions were applied at the specimens ends. Further details on the F.E. model characteristics are reported in (Gérard, Li, et al. 2019).

2.2 Characteristics of the profiles studied

Towards the assessment of global strengths of I and H-sections subject to uniform major-axis bending – some of them including high local/global coupling effects –, several hot-rolled and welded cross-section shapes leading to different values of local reduction factor χ_L and key parameter $(W_{y,el} / W_{z,el})^{0.5}$ likely to distinguish one strength curve from another were selected. Once the cross-sections geometries were chosen, eight different lengths were adopted for each specimen, so that different member slenderness λ_G could be obtained (see Eq. (2)). For each section, eight values of λ_G were sought for around $\lambda_G = [0.2; 0.3; 0.5; 0.8; 1.1; 1.4; 1.6; 2.0]$ to obtain a representative scatter distributed throughout a large range of global slenderness.

Four different yield stresses were considered ($F_y = 355MPa$, $F_y = 460MPa$, $F_y = 690MPa$ and $F_y = 770MPa$) so that further to achieve different values of χ_L, each of the eight lengths considered led to slightly different values in global relative slenderness λ_G which allowed the achievement of an exhaustive scatter. Figure 1 displays the material laws associated to each value of the yield stress.

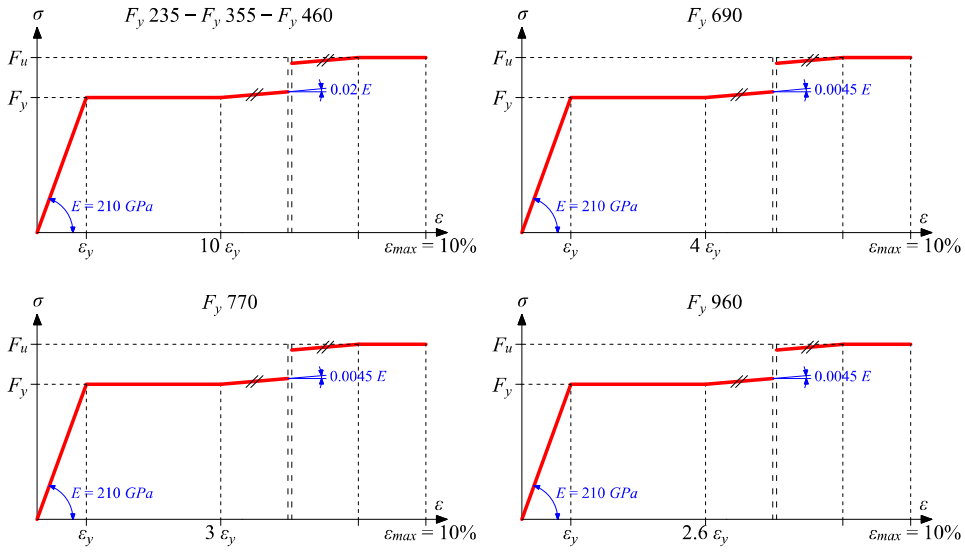

Figure 1: Material laws considered.

Table 2 reports some geometrical characteristics of the various members tested. The table specifies which sections were studied, their height-to-width ratios and their ratios of elastic section moduli.

Table 2: Characteristics associated to each cross-section considered in the present investigation.

Section	Process	h / b [-]	$(W_{y,el} / W_{z,el})^{0.5}$ [-]
IPE240	Hot-rolled	2.0	2.51
IPE300	Hot-rolled	2.0	2.54
IPE450	Hot-rolled	2.4	2.82
IPE600	Hot-rolled	2.7	3.06
HEA280	Hot-rolled	1.0	1.64
HEA500	Hot-rolled	1.6	2.18
HEA700	Hot-rolled	2.3	2.69
HEA1000	Hot-rolled	3.0	3.16
W310X28	Hot-rolled	3.0	3.31
W460X464	Hot-rolled	1.9	2.02
W690X548	Hot-rolled	2.1	2.35
W1000X350	Hot-rolled	3.3	3.34
W310X500	Hot-rolled	1.3	1.45
W310X97	Hot-rolled	1.0	1.68
W360X134	Hot-rolled	1.0	1.64
W360X744	Hot-rolled	1.2	1.38
WWF400X157	Welded	1.0	1.66
WWF500X651	Welded	1.0	1.49
WWF650X400	Welded	1.0	1.69
WWF700X175	Welded	2.3	2.69
WWF800X339	Welded	1.6	2.12
WWF350X263	Welded	1.0	1.47
IPES01S	Welded	2.2	2.84
IPES04S	Welded	2.6	3.24
IPES06S	Welded	2.0	3.00
IPES07	Welded	3.1	3.17
IPES08	Welded	3.3	3.30
IPES10	Welded	3.3	3.35
HEAS02	Welded	1.1	1.85
HEAS04S	Welded	1.1	1.88
HEAS06	Welded	1.3	2.12
HEAS08S	Welded	1.3	2.08
HEAS09S	Welded	1.1	1.92

HEAS10S	Welded	1.1	1.87

2.3 F.E. model validation against test series

Many experimental series have been carried out over the years to determine the ultimate capacities of unrestrained beams. White, Kim and Jun (see (White et Jung November 2004) and (White et Kim November 2004)) reported the main characteristics of hundreds of these tests in exhaustive reports. The reports present the results of experimental tests performed on steel I-section members under uniform bending (White et Jung November 2004) and bending moment gradient (White et Kim November 2004). To further evidence the reliability and accuracy of the F.E. model used for the consequent studies dealing with the behaviour of open-sections under constant major-axis bending, the measured parameters and initial conditions of the experimental tests were cautiously introduced into a Finite Element model.

One of these experimental investigations was carried out by Dux and Kitipornchai on hot-rolled sections in the 80's (Dux et Kitipornchai 1983). A brief yet sufficiently detailed description of the characteristics of the tests is provided in their paper. Information on material properties, geometrical and material imperfections as well as test set-up were specified which allowed a precise introduction of these parameters as input data in the F.E. model. Fork support conditions whose application method is described in (Gérard, Li, et al. 2019) were considered.

With respect to the material properties (see Figure 2), the yield strength mean values $F_{y,avg,flanges} = F_{y,f} = 285MPa$ and $F_{y,avg,web} = F_{y,w} = 321MPa$ were obtained from measurements on the flanges and web, respectively. Moreover, a Young modulus mean value $E = 209.9Gpa$ was provided. A material law including 1% of the Young modulus as strain-hardening slope was arbitrarily adopted and since neither ultimate stress nor strain were mentioned by the authors, a maximum strain $\varepsilon_{max} = 10\%$ was chosen.

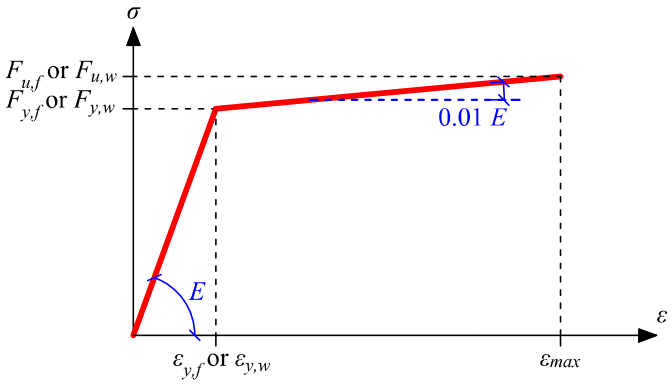

Figure 2: Constitutive law adopted for the comparison with Dux and Kitipornchai experimental tests.

Bending was applied by means of transverse loads. Three- and four-points bending tests were performed. For each bending moment distribution, several member lengths were tested. Although the test setup included a certain overhang, it was chosen to neglect their influence in the F.E. modelling. For each specimen, Table 3 reports their measured geometrical dimensions – $t_{f,avg}$ refers to the average between the thickness measured on both flanges – and associated loading set-up.

Table 3: Measured geometrical properties and loading characteristics.

	Geometrical characteristics						Loading
No. Test	$t_{f,avg}$ [mm]	t_w [mm]	b_{avg} [mm]	h [mm]	r [mm]	L [m]	
No. 1	10.6	6.6	148.1	256.2	7.5	11.0	Three-points bending

No. 2	10.7	6.8	147.6	256.4	7.5	9.0	Three-points bending
No. 3	10.6	6.6	148.5	256.1	7.5	8.0	Three-points bending
No. 4	10.6	6.6	148.5	256.1	7.5	6.0	Four-points bending
No. 5	10.6	6.8	147.7	256.3	7.5	5.0	Four-points bending
No. 6	10.7	6.8	147.6	256.3	7.5	7.0	Four-points bending
No. 7	10.7	6.8	147.6	256.3	7.5	7.0	Four-points bending
No. 8	10.6	6.8	147.7	256.3	7.5	8.0	Four-points bending
No. 9	10.6	6.8	147.7	256.3	7.5	9.0	Four-points bending

Initial bows and torsional rotations were measured prior to testing and these measurements were introduced into the numerical model by means of sinusoidal functions restrained at the load application points. With respect to material imperfections, Dux and Kitipornchai provide in (Dux et Kitipornchai 1983) the mean residual stresses values at several points of the section, obtained from measurements of residual strains through the sectioning method. A suitable triangular self-equilibrated residual stresses pattern was adopted, where an average of the maximum amplitude measured on the top flange and web was considered as magnitude of the pattern used.

Figure 3 presents the difference between experimental capacities and numerical ones obtained through G.M.N.I.A. simulations, for each of the specimens tested by Dux and Kitipornchai. On the histogram, the black dot line represents the complete adequacy between numerical and experimental results ($P_{u,F.E.} = P_{u,Exp.}$) while the red and green dot lines refer to $P_{u,F.E.} = 1.05P_{u,Exp.}$ and $P_{u,F.E.} = 0.95P_{u,Exp.}$, respectively. The figure also shows a table reporting the ratio between the ultimate capacities provided through F.E. analyses and experimental tests for each profile tested. A great adequacy between experimental and numerical resistances is highlighted on Figure 3. Further details on such F.E. model validation are reported in (Gérard 2020).

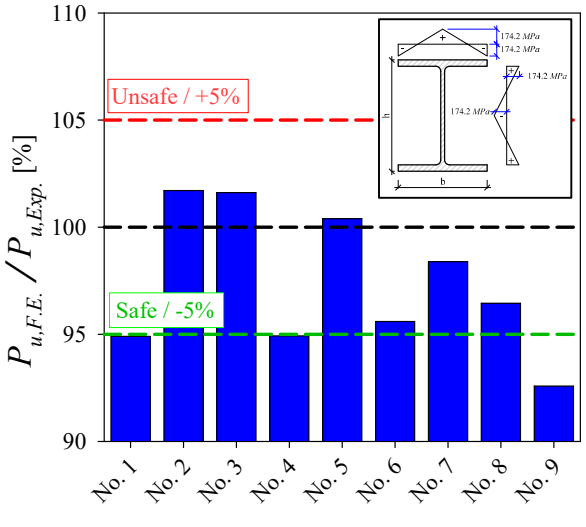

No. Test	$P_{u,F.E.} / P_{u,Exp.}$ [%]
No. 1	94.9
No. 2	101.7
No. 3	101.6
No. 4	94.9
No. 5	100.4
No. 6	95.6
No. 7	98.4
No. 8	96.4
No. 9	92.6
Average [%]	97.4
Std. dev. [%]	3.1

Figure 3: Ultimate loads achieved through F.E. simulations over the ones reached experimentally (see (Dux et Kitipornchai 1983)).

2.4 Imperfections

2.4.1 Literature study

Experimental series led to extensive measurements of global geometrical imperfections. While these imperfections represent an important parameter for a precise representation of the test into a F.E. model, their values are often source of doubts, due to the impreciseness and variability of experimental measurements. With respect to an element strength against Lateral Torsional Buckling, the initial torsional rotation and weak-axis displacements represent the key imperfections, susceptible to trigger the critical behaviour. The introduction into a F.E. model of "equivalent sets" of global lateral displacements and torsional twists as for initial imperfections – sometimes coupled with local imperfections – has already been assessed through several dedicated investigations.

The following list summarizes several studies which resulted into modelling recommendations:

- Subramanian and White (Subramanian et White 2017) recommended the use of a global geometrical imperfection introduced by means of an eigenmode shape scaled to L / 2000 at its maximum displaced node (typically at the top flange at mid-span for a beam under uniform major-axis bending) with half the residual stresses amplitudes to obtain a great agreement between experimental and numerical results. These recommendations were based on the use of the "Best-fit" of Prawel residual stresses measures (Prawel, Morrell et Lee 1974) as residual stresses pattern for welded sections and Galambos and Ketter stresses pattern (Ketter November 1958) for hot-rolled sections;
- Boissonnade and Somja (Boissonnade et Somja 2012) suggested a "reasonable" geometrical imperfection such as the 1st type of their study (see Figure 4) which included a sine-shape initial torsional twist and initial lateral displacement with a maximum of respectively L / (2000 h) and L / 1500 located at mid-span. According to their study, the use of the 1st buckling mode shape, amplified by a magnitude L / 1000, may be reliable as well. Moreover, the researchers specified that accounting for local geometrical imperfections had insignificant influence provided the section is not prone to suffer from local buckling (i.e. it does not belong to Class 4 according to EC3);

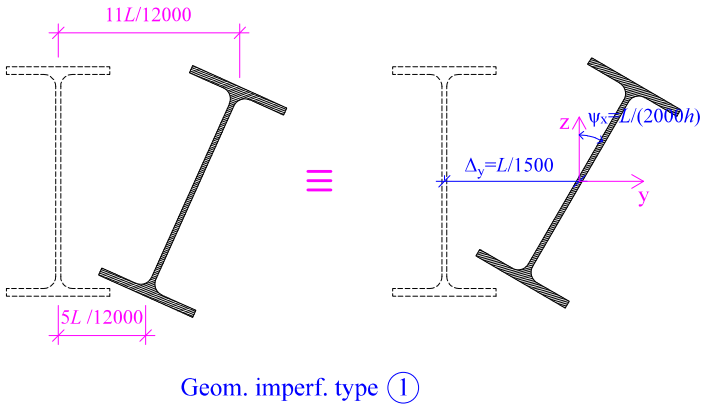

Figure 4: Type 1 imperfection pattern suggested by Boissonnade and Somja (Boissonnade et Somja 2012).

- As a result of investigations mainly carried out on flame-cut welded profiles, Thiébaud (Thiébaud 2014) proposed to use the 1st critical buckling mode shape amplified with a factor L / 1000, with 100% of the residual stresses. Then, in a different study, the author employed the 1st type suggested by Boissonnade and Somja (Boissonnade et Somja 2012) for global imperfections, associated with a local imperfection characterised by an amplitude a_i / 400 where a_i refers to the respective plate length as defined in the

Eurocode (EN 1993-1-5 2005) and a period guaranteeing square half-waves on each plate;

- Previous to his extensive investigation on the ultimate strength of open-sections under major-axis bending, Taras (Taras 2011) studied the influence of the shape and amplitude of initial imperfections on an IPE240 capacity. This preliminary study aimed at reviewing the influence of (i) the 1st lateral torsional buckling mode shape characterised by lateral displacements and torsional rotations, scaled up successively with the amplitudes $L / 2000$, $L / 1000$ and $L / 500$, (ii) a unique weak-axis displacement provided from the 1st weak-axis flexural buckling mode shape, with an amplitude $L / 1000$ and (iii) a torsional rotation obtained from the 1st critical torsional buckling mode shape;
- As part of their studies on local/global coupling behaviours under fire situations, Couto *et al.* (Couto, Vila Real et Lopes, et al. 2016) introduced some initial imperfections through eigenmode shapes. The authors studied slender sections and thus introduced into their model local geometrical imperfections by means of a local eigenmode shape. Since the Eurocode advises to use 80% of the geometrical tolerance as geometrical imperfection amplitude, the global eigenmode shape was scaled to $0.8 \cdot L / 750$ and the local one to $0.8 \cdot b / 100$ for either a maximum nodal displacement developed on the flange or $0.8 \cdot (h - 2t_f) / 100$ if achieved on the web. Then, following the Eurocode directives, the buckling mode shape (either local or global one) leading to the highest elastic critical buckling load was reduced to 70% of its initial amplitude.

This non-exhaustive list presents several ways local and global imperfections were modelled in studies whose aims were to assess the member strength with or without important local/global coupled instabilities. Different recommendations were suggested and it may be of great value to discern which one of them shall be used. Significant aspects to be noticed are that local imperfections were mostly included when one wished to specifically study local/global coupling behaviours with slender sections, whilst the absence of local geometrical imperfections is not justified for less slender sections since no actual profiles shall be free of imperfections.

2.4.2 Selection of appropriate initial imperfect shape

Subramanian and White (Subramanian et White 2017) carried out extensive studies on beams strengths and questioned the use of both full global geometrical imperfections and residual stresses typically considered in F.E. models. Nonetheless, some doubts remain since Subramanian *et al.* did not include any local imperfections in their numerical model and since the residual stresses pattern the authors suggested for welded sections is not commonly employed within the scientific community – the pattern presents different residual stresses at the web-to-flange junction.

As a main observation resulting from Couto *et al.* research (Couto et Vila Real April 2-5, 2019), the use of half the Best-fit Prawel pattern – which was suggested by Subramanian and White in (Subramanian et White 2017) – associated to local and global imperfections amplitudes of $b / 200$ and $L / 2000$, respectively, led to an upper limit for member strengths. In contrast, the pattern recommended by ECCS (ECCS-Technical Committee 8 1984) with $b / 100$ and $L / 1000$ considered as maximum amplitudes for local and global geometrical imperfections, respectively, may be considered as a lower, safe, limit.

Accordingly, results and observations presented hereafter review (i) the influence of the proportion of local imperfections considering the patterns recommended in (Gérard, Li, et al. 2019), (ii) the effects of global imperfections where global imperfections correspond to the

Type 1 suggested by Boissonnade and Somja (Boissonnade et Somja 2012) and (iii) the reduction of the usual residual stresses amplitude with the patterns suggested in (Gérard, Li, et al. 2020). A succinct comparison using experimental data as a reference is shown in the following as well.

Since the use of sine-shape imperfections allows to easily introduce both local and global imperfections into a F.E. model – which is not as straightforward when L.B.A. shapes are employed –, such sine-shape defined imperfections were employed in the present investigation.

Firstly, to provide a comparison with existent experimental data, a numerical study was performed based on the specimens tested by Dux and Kitipornchai (Dux et Kitipornchai 1983). The constitutive law and member dimensions introduced into the numerical model matched the measured ones, alike realised for the model validation. As for geometrical imperfections, since the cross-section was restrained laterally at each point load position, global imperfections showing up to 3 half-waves in the 4 points bending case were introduced. Stiffeners of 40mm thickness were arbitrarily adopted herein to guarantee the uniform distribution of the loading.

Thus, the numerical model only differed from the experimental test properties used in section 0 of this paper through the modelling of imperfections. Measured geometrical and material imperfections were replaced by the following:

- Local imperfections were set based on the recommendations made in (Gérard, Li, et al. 2019). An amplitude of a_i / 200 where a_i corresponds to each plate so-called buckling length was considered. For hot-rolled sections, the web buckling length corresponds to $a_w = h - 2t_f - 2r$ and $a_f = b - t_w - 2r$ represents the flanges one, while for welded sections $a_w = h - t_f$ and $a_f = b$ due to the absence of fillets. A half-wave length corresponding to the average between the web and flanges buckling lengths (a_f and a_w) was adopted;

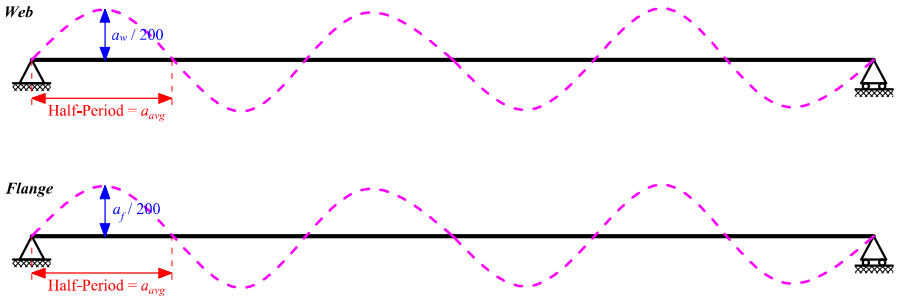

Figure 5: Local geometrical imperfections introduced into the F.E. model.

- Global imperfections matched Type 1 from (Boissonnade et Somja 2012), see Figure 4;
- Residual stresses patterns shapes and amplitudes adopted here are reported on Figure 6. Those patterns were selected subsequently to investigations providing recommendations for the introduction of material imperfections into F.E. models (see (Gérard, Li, et al. 2020)). For hot-rolled sections, the parabolic pattern was made dependent on a reference yield stress of $F_y = 235MPa$. The values $\beta = 0.30$, $\beta_1 = 0.15$ and $\beta = 0.50$, $\beta_1 = 0.25$ were considered for sections whose height-to-width ratios are above and below 1.20, respectively. Then, the remaining amplitudes were determined to guarantee plate-per-plate equilibrium ($\beta_2 = 0.075$ and $\beta_2 = 0.125$ were applied on the web compressive area to sections whose height-to-width ratios are above and below 1.20, respectively). As for welded sections whose pattern was adapted from the trapezoidal one recommended by the ECCS (ECCS-Technical Committee 8 1984), $\gamma_1 = \gamma_2 = 0.25$ were assumed.

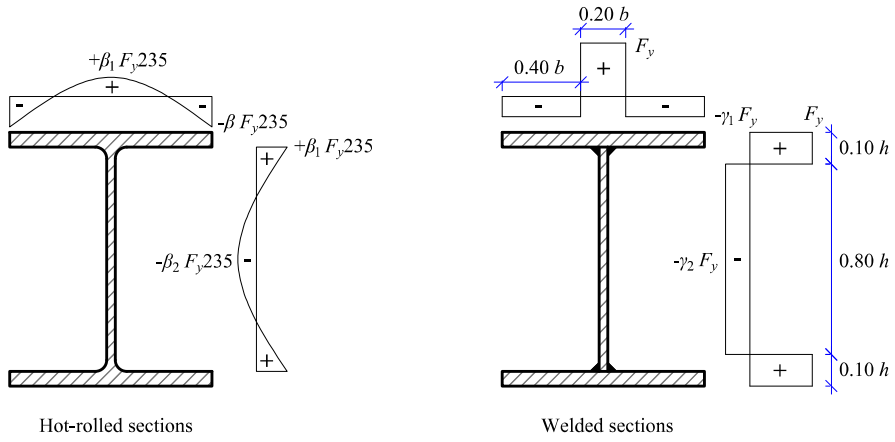

Figure 6: Residual stresses patterns considered.

As for the influence of the reduction in these imperfections' amplitude, only few possibilities were considered herein:

- The full imperfections – "100% Imp." on the figures;
- 70% of the local imperfections' amplitude coupled with 100% of the global imperfections and residual stresses – "Local 70%" on the figures;
- 70% of the global imperfections' amplitude with 100% of the local imperfections and residual stresses – "Global 70%" on the figures;
- 70% of residual stresses magnitude with 100% of geometrical imperfections – "Resi. Stress. 70%" on the figures.

Ratios between the ultimate point load obtained through F.E. simulation with distinctive imperfections amplitude over the one reached experimentally are provided on Figure 7 and Figure 8 for all specimens tested in (Dux et Kitipornchai 1983). The histogram on Figure 7 shows ultimate load ratios $P_{u,\,F.E.}$ / $P_{u,\,Exp.}$ where $P_{u,\,F.E.}$ has been obtained with the hot-rolled sections parabolic residual stresses pattern shown on Figure 6 while the equilibrated **measured** residual stresses pattern was considered to get $P_{u,\,F.E.}$ on the histogram displayed on Figure 8. Further comparisons between Figure 3 and Figure 7 shall provide an evaluation on how close the sets of imperfections (i.e. "equivalent" geometrical and material imperfections patterns) may allow to approach the experimental ultimate point load.

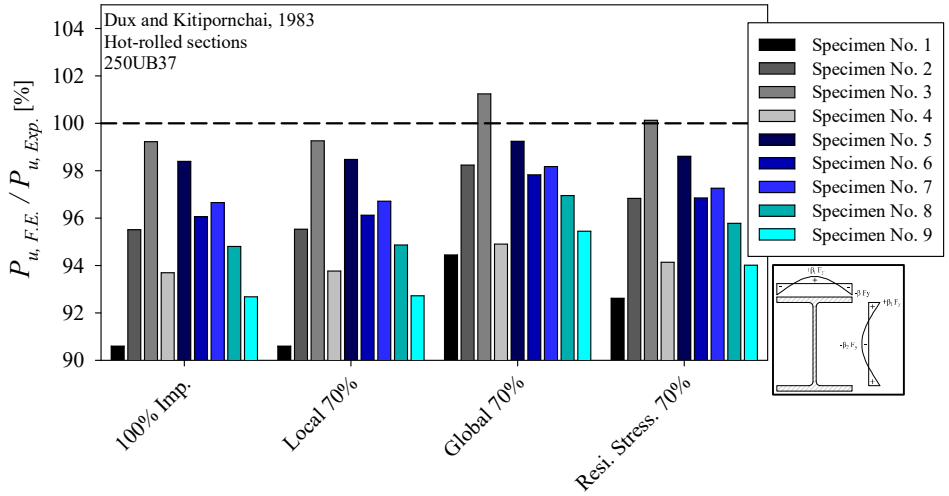

Figure 7: Imperfections amplitude influence on specimens' strength, with parabolic residual stresses.

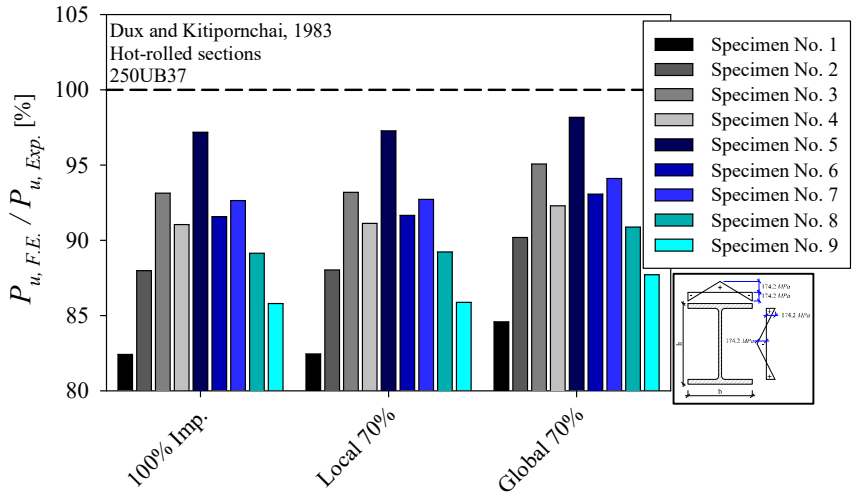

Figure 8: Imperfections amplitude influence on specimens' strength, with triangular residual stresses.

Major observations from Figure 7 and Figure 8 may be listed as follows:

- As expected, the influence of local imperfections is not significant, and does not justify a decrease in their amplitude. In addition, since a member may always present local eccentricity or out-of-straightness, regardless of its length, the use of the full local imperfections shall be recommended;
- Specimen No. 1, which is the longest one ($L = 11m$, three-points bending test), presents a significant influence of residual stresses together with specimen No. 2. At the sight of Figure 7 and Figure 8, a drop from $P_{u, F.E.} / P_{u, Exp.} = 90.6\%$ to $P_{u, F.E.} / P_{u, Exp.} = 82.4\%$ owing to the worst residual stresses measured experimentally as opposed to the "equivalent" pattern may be observed for specimen No. 1;
- As for specimen No. 5, the use of greater residual stresses has almost no effects on the specimen's predicted strength – $P_{u, F.E.} / P_{u, Exp.} = 98.4\%$ with "100% Imp." while $P_{u, F.E.} / P_{u, Exp.} = 98.6\%$ with "Resi. Stress. 70%" and $P_{u, F.E.} / P_{u, Exp.} = 97.2\%$ when measured residual stresses are considered. With respect to the influence of global imperfections amplitude (see Figure 7), a nearly negligible difference of 1% in ratios $P_{u, F.E.} / P_{u, Exp.}$ may be observed. Specimen No. 5 is the shortest one ($L = 5m$) and presents the shorter unrestrained spans since the loading situation corresponds to a four-points bending, making it more compact than the others which may explain a little sensitivity to geometrical and material imperfections;
- Overall, great strength predictions were reached when 70% of the global imperfections were introduced into F.E. models. For specimen No. 1, while the agreement between ultimate capacity reached experimentally and numerically is still lower than the one obtained when the "measured" imperfections are considered, it may still be closely approached with 70% of the global imperfections. The agreement reached may even be better than the one obtained with the measured imperfections, as seen for specimen No. 6 and specimen No. 9 using 70% of the global amplitude. Then, for the others except specimen No. 2, insignificant differences were obtained between the correlations reached.

To deepen this investigation, further numerical series were carried out on three distinctive section shapes as well as several member lengths. Two hot-rolled sections, W1000X883 and HEA300 as well as one welded section *IPES* – beam shape with thin web – were tested under uniform major-axis bending. In the following graphs, L_1 refers to the most compact elements

while L_4 represents the most slender ones. For the imperfections patterns, the same sine-shape equations and residual stresses patterns as those considered throughout the comparison with experimental capacities were assumed. The material law described on Figure 1 with a yield strength $F_y = 355MPa$ was introduced in the F.E. models. Finally, similar boundary conditions and loading method as those described in (Gérard, Li, et al. 2019) were considered at the member ends.

Several proportions of each imperfections – local geometrical, global geometrical or residual stresses – amplitudes were tested. Figure 9, Figure 10 and Figure 11 display the ultimate major-axis bending strength $M_{y,u}$ reached with each specific case considered, over the one where the full imperfections amplitude has been applied $M_{y,u,100\%}$ (i.e. 100% of local imperfections recommended in (Gérard, Li, et al. 2019), 100% of Type 1 imperfections suggested by Boissonnade and Somja in (Boissonnade et Somja 2012) and 100% of the residual stresses pattern amplitudes shown on Figure 6).

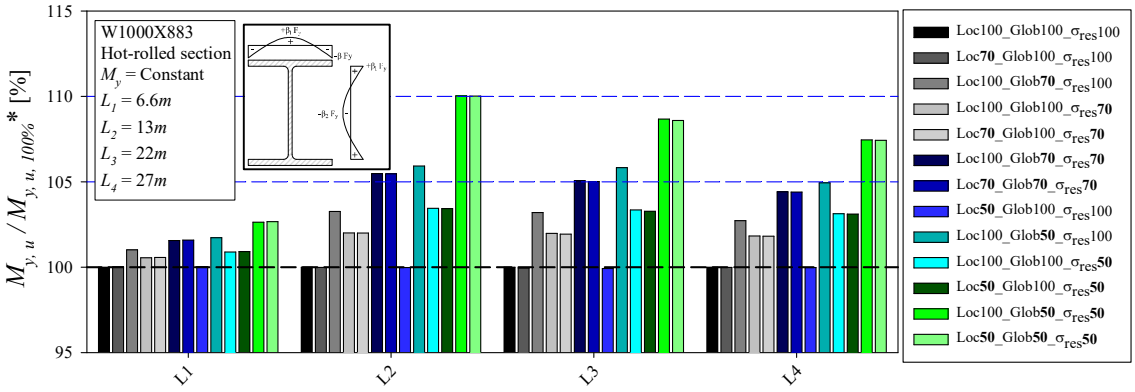

*$M_{y,u,100\%} = M_{y,u}$ with 100% local imperfections, 100% global imperfections, 100% residual stresses (Case Loc100_Glob100_σ_{res}100)

Figure 9: Imperfections amplitude influence on the resistance of a W1000X883 made of F_y355 steel.

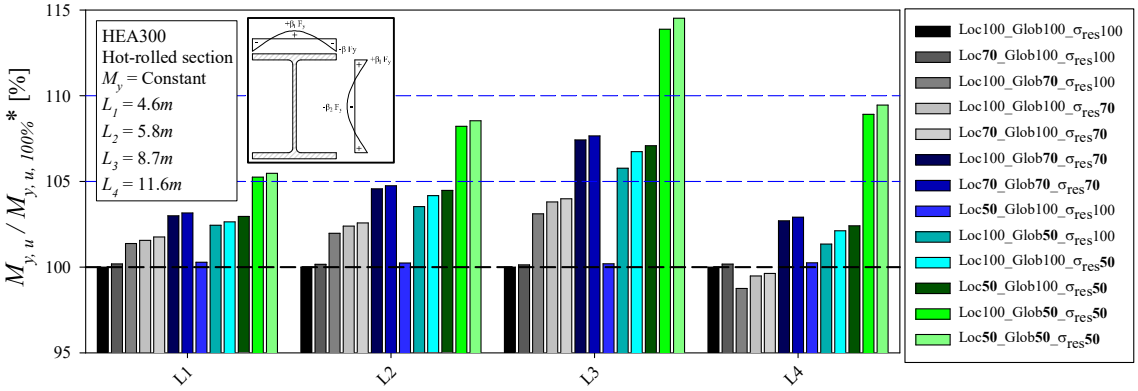

*$M_{y,u,100\%} = M_{y,u}$ with 100% local imperfections, 100% global imperfections, 100% residual stresses (Case Loc100_Glob100_σ_{res}100)

Figure 10: Imperfections amplitude influence on the resistance of a HEA300 made of F_y355 steel.

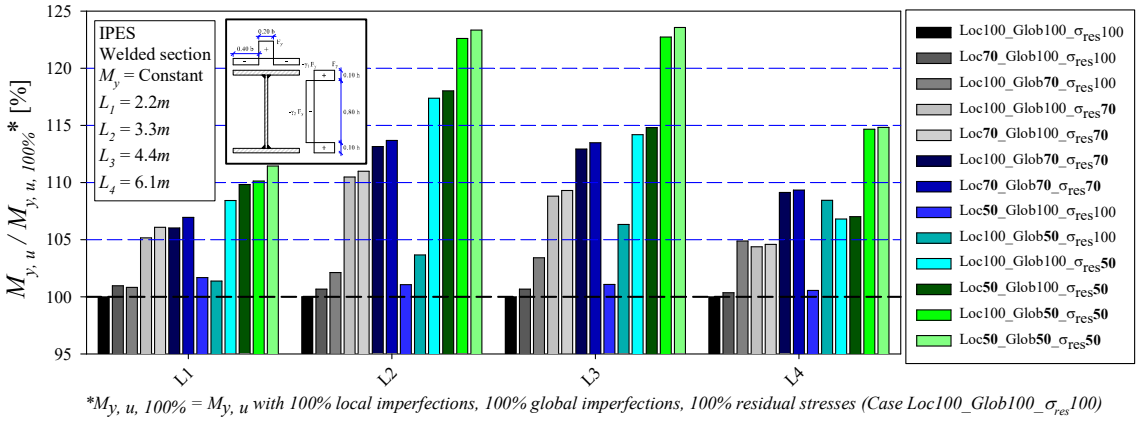

$M_{y,u,100\%}$ = $M_{y,u}$ with 100% local imperfections, 100% global imperfections, 100% residual stresses (Case Loc100_Glob100_σ_{res}100)

Figure 11: Imperfections amplitude influence on the resistance of an invented section, *IPES* made of F_y355 steel.

As a first obvious observation, the influence of local imperfections remains quite reasonable and tends to be nearly invisible in most cases. The welded section *IPES* – which belongs to Class 4 due to its high local slenderness –, shows a low but yet existent strength increase when lower local amplitudes are used for a short member whose failure is governed by local behaviour. Thus, since local imperfections are still likely to exist in a "real" manufactured element, there are no reason to remove them. When failure occurs locally, their presence is quite relevant as well as when the failure involves strong local/global couplings. Moreover, their low influence on the strength does not justify any decrease in their amplitude and they shall not be lowered in any extent.

Then, as a general observation on the influence of global imperfections, their decrease may lead to up to an 8% strength increase within the intermediate global slenderness range – with 50% reduction in their amplitude. This strength raise is obtained with the longest span L_4 considered for a welded *IPES* which corresponds to a global relative slenderness $\lambda_G \approx 1.3$.

Except for L_4, a lower level of residual stresses is seen to have a greater influence on *IPES* than a decrease in global imperfections amplitude. Further, while the influence of a drop in the residual stresses magnitude has a significant impact on the strength of welded slender *IPES*, it does not influence hot-rolled sections capacities in such great extent: a higher positive influence on the resistance is highlighted when global imperfections' amplitude is reduced than with residual stresses reduction for the hot-rolled W1000X883 while similar strengths are obtained with either a decrease in global imperfections or residual stresses for hot-rolled HEA300.

The unique decrease in residual stresses amplitude results into a 17% strength gain for an *IPES*, even for a short member whose strength may be raised by up to 10%, less than 5% gain for a hot-rolled W1000X883 and 6% for the hot-rolled HEA300. Important to be noticed here is that the effects of a combination of the decrease of the proportion of several imperfections' amplitudes was seen to allow for up to 23% strength gain for a welded *IPES* once both global geometrical imperfections and material imperfections were lowered, which is quite significant. Nonetheless, no experimental data may confirm these higher strengths for slender welded sections so that it may be over favourable to apply such drastic imperfections amplitude reduction.

Even with these sets of imperfections which were seen to be quite higher compared to those measured on the specimens (Gérard 2020), close estimate of the tests capacities could be reached. With respect to Dux and Kitipornchai experimental series, while the researchers did not measure such geometrical imperfections' magnitudes, the residual stresses from their

measurements were much higher than the ones usually measured on hot-rolled sections. Since the purpose is here to determine suitable sets of imperfections which may be applicable for all situations, estimate of peak load predictions may be more useful than a strict comparison with measured imperfections.

In view of the observations resulting from the comparison with experimental data and from the analyses of pure F.E. results, the main conclusions of this study are as follows:

- Since *local* imperfections were carefully adopted as a result of a comprehensive study on short members (see (Gérard, Li, et al. 2019) and (Gérard 2020)) and comparisons with local experimental ultimate capacities were made, keeping 100% of their amplitude seems like a reasonable suggestion. In addition, it was evidenced that these imperfections have an influence only on slender sections and that they definitely need to be included to account for high local behaviour. Otherwise these imperfections have insignificant influence in most cases;
- Residual stresses result from the manufacturing process and the magnitude of the patterns were adopted after deep comparisons with experimental data and consecutive numerical series were then performed to test several of the patterns mentioned in (Gérard, Li, et al. 2020). Decreasing their amplitude even though they are actually present on the profile may seem unjustifiable;
- Decreasing the global imperfections amplitudes to 70% of their initial value (Type 1 suggested in (Boissonnade et Somja 2012)) represents a fair option to reach close strength estimates predicted experimentally.

Through a $\chi_G - \lambda_G$ format (see Eqs. (1) and (2)), Figure 12 depicts the global strengths numerically predicted for the three sections studied in the present investigation – for all cases considered on Figure 9, Figure 10 and Figure 11. The figure is displayed in a so-called O.I.C. format. The O.I.C. relies on the use of load multipliers which allows to use one same concept for both simple and combined loadings (see (Boissonnade, et al. 2017)). Therefore, through the use of such load multipliers, an O.I.C. graph displays the global reduction factor χ_G – which if applied to the reduced plastic capacity owing to local buckling effects leads to the ultimate capacity – as a function of the global relative slenderness λ_G. The definitions of χ_G and λ_G are reported in Eqs. (1) and (2), in which M_{ult} refers to the ultimate bending moment, M_{pl} represents the plastic bending moment and M_{cr} corresponds to the elastic critical buckling bending moment. χ_L refers to the local reduction factor, reducing the plastic capacity owing to local buckling.

$$\chi_G = \frac{M_{ult}}{\chi_L \cdot M_{pl}} \tag{1}$$

$$\lambda_G = \sqrt{\frac{M_{pl}}{M_{cr}}} \tag{2}$$

In addition, the figure exhibits capacities obtained with the adopted imperfections (i.e. 100% of local amplitude, 70% of global amplitude and 100% of residual stresses magnitude) through the multi-linear curves. As for the welded section *IPES*, two curves may be distinguished based on different proportions of imperfections: "IPES_Loc100_Glob100_σ_{res}70" corresponds to the unique decrease in residual stresses magnitude while case "IPES_Adopted_imp." refers to the

proportions finally chosen where only 70% of global amplitudes are introduced while other imperfections amplitudes remain unchanged.

As pointed out by several authors the past few years such as Couto *et al.* (Couto et Vila Real April 2-5, 2019) and Trahair (Trahair 1993, ISBN 0-8493-7763-3), an unexpected significant decrease (see red ellipse on Figure 12) in member strengths of welded sections may occur for specific residual stresses patterns. Trahair suggested that this abrupt strength reduction could be attributed to the more detrimental shape of the residual stresses pattern.

As a result of Couto investigations (Couto et Vila Real April 2-5, 2019), the following was observed:

- The ECCS pattern (see (ECCS-Technical Committee 8 1984)) leads to the lowest strengths and the sudden strength drop for welded I-shapes is the most pronounced if such pattern is introduced;
- Boissonnade *et al.* pattern shown on Figure 6 (also named as "Taras" pattern in (Couto et Vila Real April 2-5, 2019), see Figure 6) leads to quite similar strengths than the "Best-fit Prawel" (see (Subramanian et White 2017)) except for global relative slenderness below 0.75 where it exhibits a sudden drop of strength – although in a lower extent than the ECCS pattern;
- The ECCS pattern is more conservative than the Boissonnade *et al.* pattern for the range of global slenderness $0.75 < \lambda_{LT} \leq 1.5$;
- The responsibility of the presence of a constant rectangular block of compressive residual stresses at flanges tips on the drop of strength at low to intermediate member slenderness is not strictly evidenced since non-linear results based on "Clarin" pattern – which exhibits similar residual stresses distribution (although with different amplitudes), see (Couto et Vila Real April 2-5, 2019) – do not present the abrupt strength decrease specified above.

As shown on the graph, decreasing the magnitude of residual stresses (see curve "IPES_Loc100_Glob100_σ_{res}70" on the graph) does not allow for the disappearance of the plateau – although no experimental data may neither support nor refute the existence of such plateau for now.

As expected, the adoption of lower amplitudes for global geometrical imperfections results into higher strengths mostly within the intermediate slenderness range. While the scatter of results is the sparsest for global relative slenderness λ_G ranging from 0.8 up to 1.3 for hot-rolled sections, the influence of imperfections seems still pronounced even at low slenderness for the welded *IPES*. As shown on Figure 11, the influence of global imperfections has almost no impact on the welded section strength at low slenderness and this great scatter may be mainly attributed to the decrease in residual stresses magnitude.

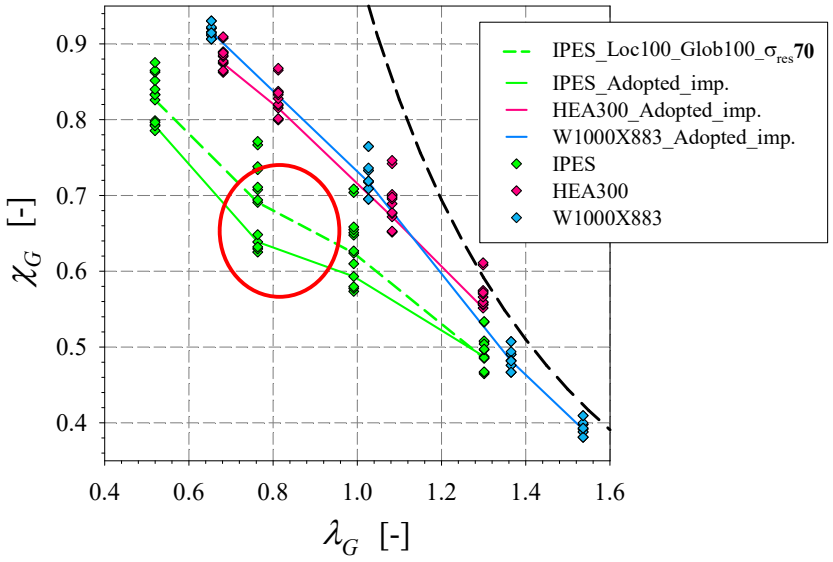

Figure 12: Influence of imperfections on global strengths.

2.5 F.E. model prevented from local buckling occurrence

First comprehensive series of numerical simulations were performed by means of the shell F.E. model described in (Gérard, Li, et al. 2019).

To study the influence of local buckling on beams overall behaviour, a subsequent F.E. model prevented from the occurrence of any local instabilities was developed, based on a study carried out by Beyer (Beyer 2017). As suggested by Beyer (Beyer 2017), some additional rigid elastic beam elements were introduced between each "strip" of shell elements so that sufficient bending stiffness could be provided to the web and flanges (see Figure 13b) to prevent them from local buckling. A parametric study was first carried out to determine which properties shall be adopted for those beam elements.

As recommended by Beyer the reference stiffness adopted were set based on each plate slenderness limit (between Class 1 and Class 2 sections) provided by the Eurocode for plates subject to uniform compression. Eq. (3) provides the reference stiffness suggested for webs while Eqs. (4) defines the reference stiffness adopted for the flanges, where l_{shell} represents the length of shell elements along the longitudinal axis of the profile.

$$E_{beam,web} \cdot I_{beam,web} = 10 \cdot \frac{E_{profile} \cdot \left({h_w}/{33\varepsilon}\right)^3}{12(1-\nu^2)} l_{shell} \tag{3}$$

$$E_{beam,flange} \cdot I_{beam,flange} = 10 \cdot \frac{E_{profile} \cdot \left({0.5 \cdot b}/{9\varepsilon}\right)^3}{12(1-\nu^2)} l_{shell} \tag{4}$$

A unique and reasonably low value of b was adopted while beams height was determined following the definitions of $I_{beam,web}$ and $I_{beam,flange}$ based on a Young modulus $E_{beam,flange} = 100 \cdot E_{profile}$. Figure 13 exhibits the deformed shape obtained at peak load for a welded IPES04S (see Table 2) with influence of local buckling (Figure 13a) and without any local buckling effects (Figure 13b).

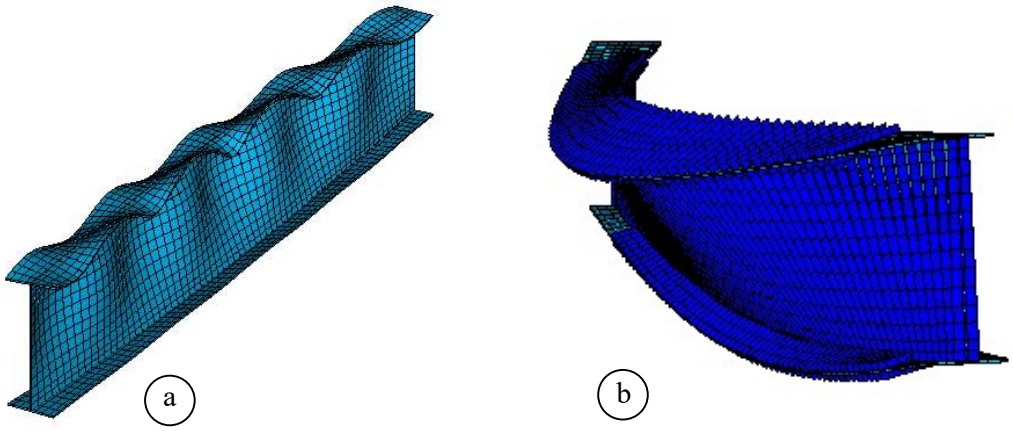

Figure 13: Deformed shape at peak load of a welded IPES04S.

3. Member resistance predictions for hot-rolled and welded sections

3.1 Design proposal

3.1.1 Basis of the design proposal

The design approach suggested through the O.I.C. resorts to the well-known notion of load multipliers. It allows to use one concept for both simple and combined loadings and avoid the use of interaction equations. All load multipliers for a same situation are coupled with a same initial loading. They are easy to use, and provided the initial load has been wisely chosen, the load multipliers shall remain in a same range of values allowing for a same automatic convergence criterion. For instance, if a beam whose plastic bending moment is $M_{pl} = 759kN.m$ is subjected to a major-axis bending $M_{y,Ed} = 92.25kN.m$, the load multiplier R_{pl} associated to the plastic capacity shall be $R_{pl} = M_{pl} / M_{y,Ed} = 8.228$. Furthermore, load multiplier $R_{b,L+G}$ refers to the ultimate bending moment including local and global buckling effects. Once multiplied by the applied loading $M_{y,Ed}$, the ultimate bending moment $M_{ult} = R_{b,L+G} \cdot M_{y,Ed}$ may be achieved. On the other hand, load multiplier $R_{b,G}$ is attained with a member prevented from the occurrence of local buckling, i.e. using the F.E. model displayed on Figure 13b.

An O.I.C.-type design curve is based on a modified version of the Ayrton-Perry base equation (Ayrton et Perry 1886). For the formulation to present more adaptability and be suitable for all load cases and geometries, additional non-constant parameters were introduced into the definitions of χ and ϕ suggested by Ayrton and Perry, as Eqs. (5) and (6) show.

$$\phi = 0.5\left(1 + \alpha_G(\lambda_G - \lambda_0) + {\lambda_G}^{\delta}\beta\right) \tag{5}$$

$$\chi_G = \frac{1}{\phi + \sqrt{\phi^2 - {\lambda_G}^{\delta}\beta}} \tag{6}$$

In Eqs. (5) and (6), the expressions of β, α_G, λ_0 and δ depend on the leading parameters identified and characterised within the present investigations. β enables to consider benefits from strain-hardening while α_G stands for the influence of imperfections. λ_0 corresponds to the end of the plastic plateau and δ allows to account for post-buckling strength.

3.1.2 Determination of a local/global coupling function

- Hot-rolled sections

Towards the development of a local/global coupling function accounting for the variation of local buckling influence with the member slenderness, Figure 14 shows ratios $R_{b,L+G} / R_{b,G}$ as functions of the global relative slenderness. Such ratios highlight the proportion of local buckling influence and local/global coupling effects on the overall member strength.

The several points may be attributed to different values of local reduction factors reached numerically so that the influence of local buckling on the member strength may be evaluated.

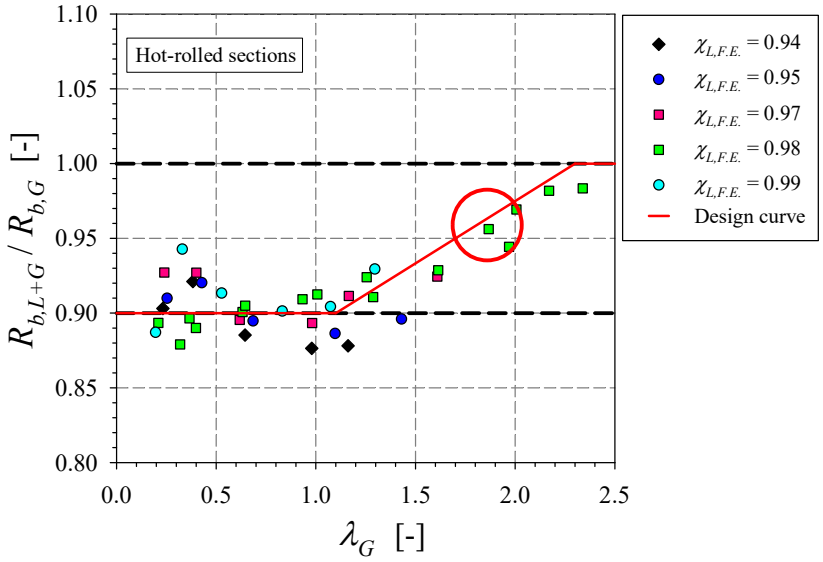

Figure 14: Influence of local effects and local/global interactions on the member strength for hot-rolled sections.

To obtain an equation of the local/global coupling function based on the numerical results of ratios $R_{b,L+G} / R_{b,G}$, the starting and ending λ_G values of the linear segment indicating the transition from the full influence of local effects up to the removal of such influence for high global slenderness were kept. Values of ratio $R_{b,L+G} / R_{b,G}$ reached on short elements were replaced by $f_{L/G} = 1.0$, so that the full influence of local buckling was considered for such members. While the λ_G values where the decrease in local buckling influence begins and ends were chosen in agreement with Figure 14, the slope of such drop was not respected in the following definition of $f_{L/G}$.

Based on those assumptions, Figure 15 depicts the design equation chosen for the local/global coupling function so that the overall tendencies obtained on Figure 14 are respected. The equation suggested for the local/global coupling function $f_{L/G}$ for hot-rolled sections is presented in Table 4. The following was considered:

- The full influence of local buckling is kept at low global relative slenderness – i.e. $f_{L/G} = 1.0$;
- For values of χ_L higher than 1.0, $f_{L/G} = 1.0$ is suggested whatever the global relative slenderness value;
- Same λ_G limits of the decrease in local influence are adopted for all local reduction factors considered;
- The local/global coupling function is still made dependent on the local reduction factor χ_L since it should have fewer effect for values of χ_L close to 1.0 (see Table 4);
- The influence of local buckling is removed (see the final plateau of $f_{L/G}$ on Figure 15) at high global relative slenderness since those members mostly fail owing to lateral torsional buckling.

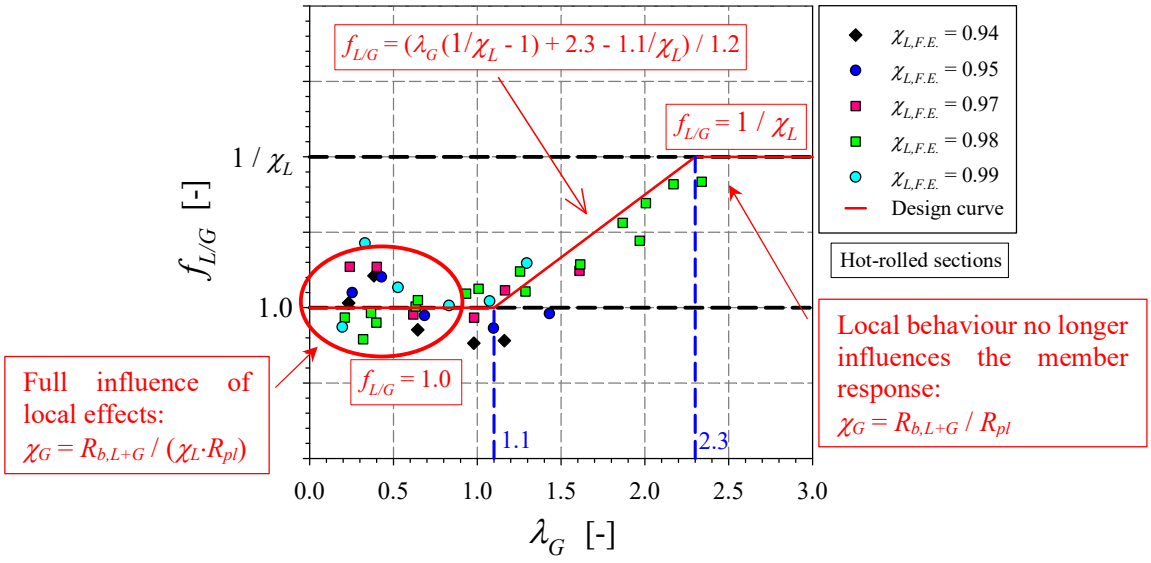

Figure 15: Derivation of the local/global coupling function $f_{L/G}$ for hot-rolled sections.

Table 4: Proposed formulation of the local/global coupling function $f_{L/G}$ for hot-rolled sections.

$\lambda_G < 1.1$	$f_{L/G} = 1.0$
$1.1 < \lambda_G < 2.3$	$f_{L/G} = \dfrac{\lambda_G\left(\frac{1}{\chi_L} - 1.0\right) + 2.3 - 1.1\frac{1}{\chi_L}}{1.2}$
$\lambda_G > 2.3$	$f_{L/G} = 1.0 / \chi_L$

Following the O.I.C. approach, the local/global coupling function $f_{L/G}$ was then introduced into the definition of χ_G, as defined in Eq. (7), so that F.E. points could be added to the $\chi_G - \lambda_G$ graph (see Figure 18).

$$\chi_G = \frac{R_{b,L+G}}{\chi_L \cdot R_{pl} \cdot f_{L/G}} \tag{7}$$

- Welded sections

As for the design of welded sections, a similar approach was followed, and a definition of $f_{L/G}$ was established based on the tendencies observed on Figure 16. The large influence of the presence of local behaviour on the member response may be observed on the figure which displays $R_{b,L+G}$ to $R_{b,G}$ ratios as a function of the global relative slenderness λ_G for several local reduction factors χ_L. Unlike the tendencies observed for hot-rolled sections, results show a large influence of the local reduction factor even at high member slenderness where some local buckling effects still remain.

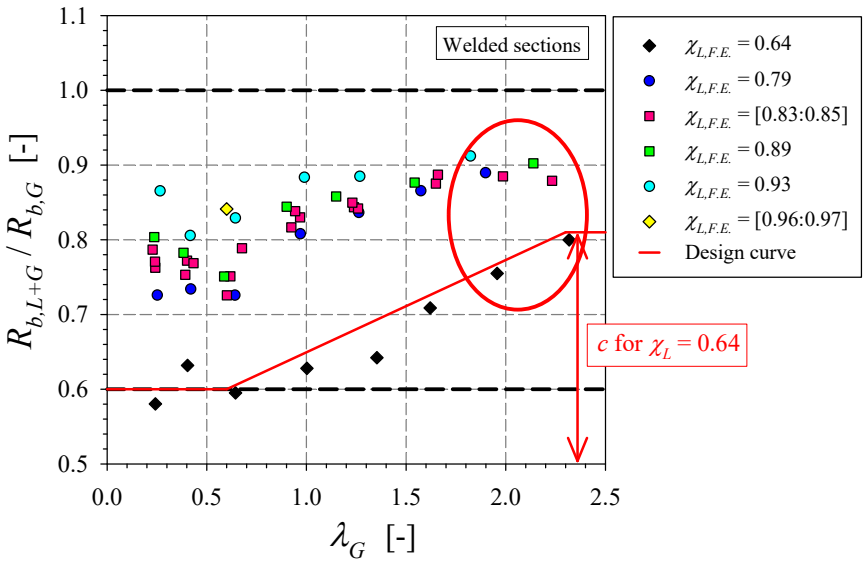

Figure 16: Influence of local effects and local/global interactions on the member strength of welded sections.

Figure 17 depicts the local/global coupling function $f_{L/G}$ as a function of the global relative slenderness for different values of the local reduction factor reached with welded sections. In contrast with the formulation chosen for hot-rolled sections, the λ_G limit ($\lambda_{G,02}$ in Table 6) – standing for the boundary between the decrease in local buckling influence and the final plateau reached – was made dependent on the local reduction factor χ_L. Further to that, an additional parameter c was introduced in the design so that the final proportion of local effects still acting on the overall member response also rely on χ_L as a result of observations made on ratios $R_{b,L+G}$ / $R_{b,G}$. As shown on Figure 16, values of parameter c were adopted based on the final plateaus of ratios $R_{b,L+G}$ / $R_{b,G}$ reached at high λ_G – thus directly reflecting the remaining influence of local buckling at high member slenderness. The value of c selected for a local reduction factor χ_L = 0.64 is reported on Figure 16.

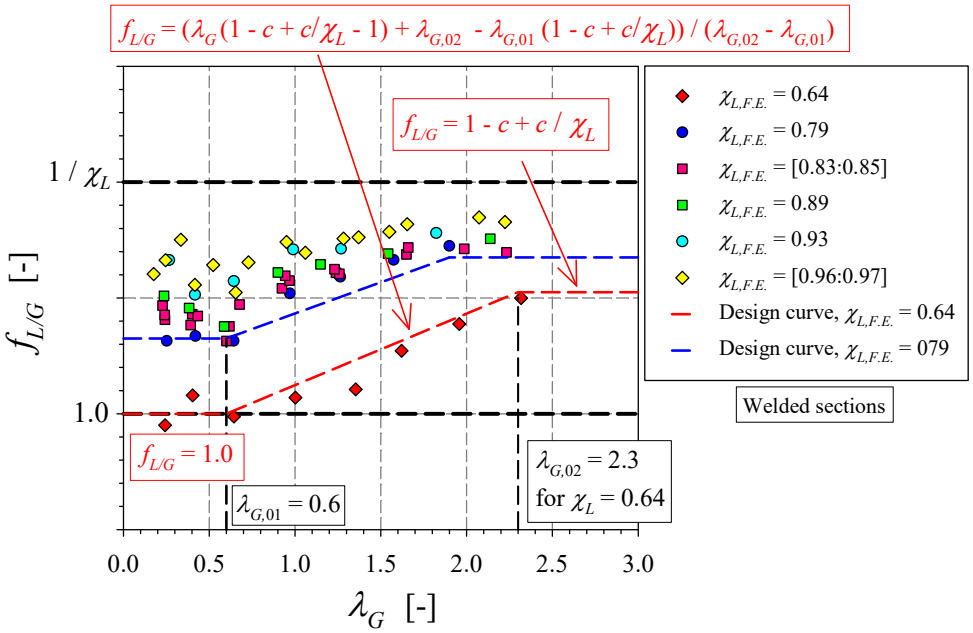

Figure 17: Derivation of the local/global coupling function $f_{L/G}$ for welded sections.

Table 5 presents the design formulation chosen for $f_{L/G}$ while definitions of the parameters used within the equation of the local/global coupling function are presented in Table 6.

Table 5: Formulation of the local/global coupling function $f_{L/G}$ for welded sections.

$\lambda_G < \lambda_{G,01}$	$f_{L/G} = 1.0$
$\lambda_{G,01} < \lambda_G < \lambda_{G,02}$	$f_{L/G} = \frac{\lambda_G \left(1 - c + \frac{c}{\chi_L} - 1\right) + \lambda_{G,02} - \lambda_{G,01} \left(1 - c + \frac{c}{\chi_L}\right)}{\lambda_{G,02} - \lambda_{G,01}}$
$\lambda_G > \lambda_{G,02}$	$f_{L/G} = 1 - c + c / \chi_L$

Table 6: Definitions of parameters used in the local/global coupling function for welded sections.

$\lambda_{G,01}$ [-]	0.6
$\lambda_{G,02}$ [-]	$-2.17 \cdot \chi_L + 3.66$
c [-]	$0.42 \cdot \chi_L + 0.54$

3.1.3 Design proposal for hot-rolled sections

Strength curves were then eventually derived. In a $\chi_G - \lambda_G$ format, Figure 18 shows both the F.E. results associated to different ranges of ratios $(W_{y,el} / W_{z,el})^{0.5}$ and a set of strength curves as lower bounds of some of these ranges.

Values of the local reduction factor used for the determination of χ_G (see Eq. (7)) correspond to the ones predicted through non-linear analyses – meaning neither the O.I.C. proposal nor some standard's proposal were used. If so ever the local reduction factor exceeded 1.0 – i.e. strain-hardening begins to have some influence and higher strengths than the plastic one were achieved – values of χ_L were replaced by 1.0. This shall explain why some results lie above the upper limit $\chi_G = 1.0$

Global reduction factors higher than 1.0 were achieved with compact to very compact cross-sections so that such short members presented important strain-hardening effects. All the results presenting ratios χ_G above 1.0 did present local reduction factors above 1.0 as well. While a lower amount of strain-hardening benefits is highlighted at the "global" level for such compact sections, they still present up to 4% strength gain as pointed out on the figure. As for sections whose local reduction factors χ_L were below 1.0, local effects were removed through χ_L in χ_G definition so that only the global ones remained.

The influence of the section strong to weak-axis yield moduli ratio is shown on Figure 18. Results depict a more direct tendency with ratio $(W_{y,el} / W_{z,el})^{0.5}$ than what was observed with h / b in (Gérard 2020). The higher is the ratio $(W_{y,el} / W_{z,el})^{0.5}$, the lower are the global strengths reached. Moreover, scatters for similar $(W_{y,el} / W_{z,el})^{0.5}$ ratios are quite narrow and allow for the formulation of a unique buckling curve.

However, more complex tendencies are highlighted at some members slenderness:

- For λ_G about 1.0, the scatter owing to a ratio $(W_{y,el} / W_{z,el})^{0.5} = [1.6:1.7]$ (dark blue points) expands;
- For λ_G from 1.5 to 2.5, sections whose $(W_{y,el} / W_{z,el})^{0.5} = [1.6:1.7]$ (dark blue points) show higher global strengths than sections with a ratio $(W_{y,el} / W_{z,el})^{0.5}$ within the range [1.4:1.5] unlike the overall tendencies. This global slenderness range may be potentially influenced by both strain-hardening effects – since the member is subjected to

minor-axis bending due to the large torsional rotations it experienced – and global post-buckling strength.

For long elements made of H-shapes, benefits from strain-hardening may become relevant at high λ_G. Indeed, such sections were seen to suffer from large torsional twists at high global relative slenderness. For H-shapes with compact flanges, some strain-hardening benefits may thus appear if their local reduction factor reached on a short element subjected to minor-axis bending exceeds 1.0. H-sections presenting such local reduction factor below 1.0 shall be governed by local buckling of their flanges at high global slenderness.

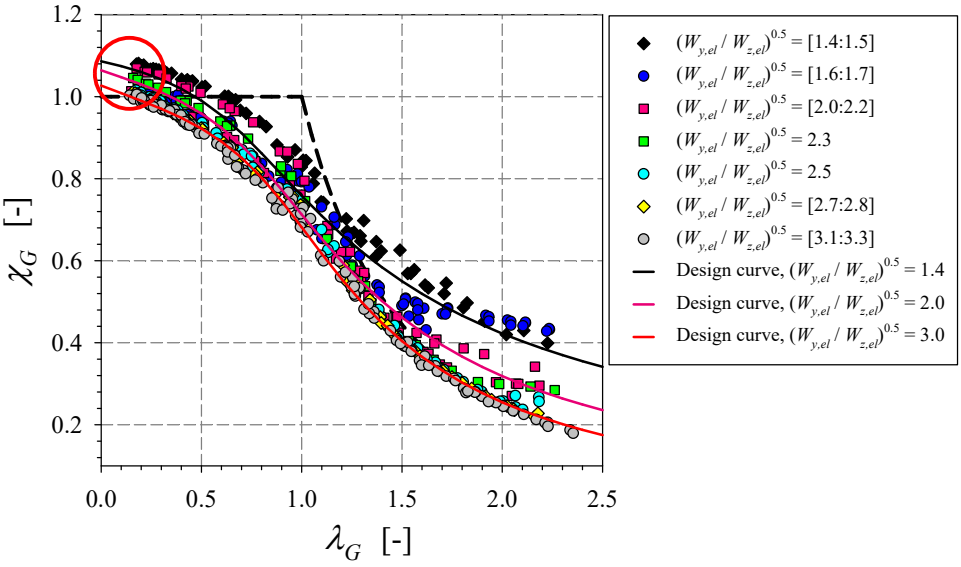

Figure 18: Design proposal and F.E. results for the global strength of hot-rolled sections.

Design curves shown on Figure 18 follow the O.I.C. approach and are based on a modified version of Ayrton-Perry formulation (see paragraph 0). Table 7 reports the definition of parameters used within the design formulation β, δ, α_G and λ_0, which were made dependent on ratio $(W_{y,el} / W_{z,el})^{0.5}$. For values of $(W_{y,el} / W_{z,el})^{0.5}$ above 3.0, $(W_{y,el} / W_{z,el})^{0.5} = 3.0$ shall be used, i.e. $(W_{y,el} / W_{z,el})^{0.5} = 3.0$ may be considered as the lower bound of the global strength curves.

Table 7: Definition of parameters considered in the formulation for global design of hot-rolled sections.

	For $\lambda_G > 0$
β	$-0.039\ (W_{y,el} / W_{z,el})^{0.5} + 1.11$
δ	$-0.23\ (W_{y,el} / W_{z,el}) + 1.50\ (W_{y,el} / W_{z,el})^{0.5} - 0.63$
α_G	$-0.023\ (W_{y,el} / W_{z,el}) + 0.144\ (W_{y,el} / W_{z,el})^{0.5} - 0.041$
λ_0	0.2

Further studies are required to sought for a design proposal for welded sections.

3.2 Accuracy of the design proposal and comparison with existing codes provisions

A comparison between the accuracy of the strength predictions reached with the O.I.C. and Eurocode proposals is shown on Figure 19. The figure displays ratios $\chi_{G,Ref.} / \chi_{G,F.E.}$ as functions of the member slenderness λ_G where *Ref.* refers either to the O.I.C. or the Eurocode.

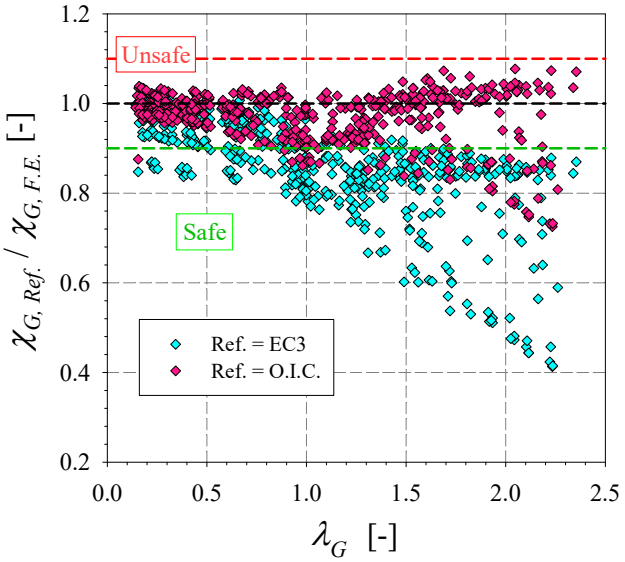

Figure 19: Efficiency of the Eurocode design provisions and O.I.C. proposal.

Although the strengths predictions achieved with the O.I.C. proposal begin to lose in accuracy compared to F.E. results at high member slenderness, overall the proposal provides reasonable estimate of numerical strengths. In comparison, resistances estimated through the Eurocode show poor accuracy and ratios $\chi_{G,Ref.}$ / $\chi_{G,F.E.}$ as low as 0.40 are reached. Nonetheless, it is important to notice that such ratios correspond to column shapes experiencing high torsional twists – not considered through the Eurocode – and may not correspond to actual applications.

4. Conclusions

The present study focused on the global strength of hot-rolled and welded I and H-shapes subjected to uniform major-axis bending. The paper aimed at providing a pertinent method to assess local/global coupling behaviours through a unique design proposal.

With the increased use of high strength steel, a more efficient design of slender sections would allow for important material savings. The shortcomings highlighted by the codes with respect to the design of beams made of slender sections were evidenced in section 0 of this paper.

A preliminary study including some comparisons with experimental ultimate capacities was carried out to determine a reasonable initial imperfect shape. Then, some numerical series were performed on I and H-shapes with several member lengths to investigate the extent of local/global interactions. In that context, a F.E. model was developed to prevent any local buckling occurrence so that purely global ultimate strengths could be achieved.

After a careful assessment of the F.E. model reliability through a comparison with experimental data, investigations on the influence of local and global geometrical imperfections as well as residual stresses allowed the determination of a reasonable pattern. The use of local geometrical imperfections recommended in (Gérard, Li, et al. 2019) characterised by an amplitude applied a_i / 200 per plate and a half-wave length corresponding to the average between the web and flanges so-called buckling lengths (a_f and a_w) and of the residual stresses patterns suggested in (Gérard, Li, et al. 2020) and shown on Figure 6 together with a decrease to 70% of the "type 1" global geometrical imperfections used in (Boissonnade et Somja 2012) were suggested. However, as observed and mentioned previously by several researchers, a strength drop was highlighted for welded sections and further research may be required to determine the veracity of such behaviour.

As a result of numerical studies, some local/global coupling functions were then established for hot-rolled and welded sections based on a comparison between results achieved with two different F.E. models – one including the influence of local buckling and the other one providing the pure global strength – so that the variation of participation of local effects on the overall strength could be assessed.

For hot-rolled sections, this function ruling the local/global coupling behaviour was derived and introduced in χ_G definition – and also in the final verification – to decrease the influence of χ_L together with the raise of global relative slenderness λ_G. A final design proposal governing $\chi_G - \lambda_G$ relationship and describing as close as possible the strengths tendencies observed was then established whose agreement with F.E. capacities showed great concordance compared to what achieved with the Eurocode. Compared to current standards provisions and most recent researches carried out on the subject, such design proposal presents the benefits to be continuous between doubly-symmetric sections geometries.

As for welded sections, a reliable and pertinent formula ruling local/global coupling behaviours through a unique function $f_{L/G}$ was derived and made dependent on the local reduction factor χ_L describing the sensitivity of the cross-section to suffer from local buckling under uniform major-axis bending. However, no design proposal ruling the $\chi_G - \lambda_G$ relationship could be established.

The O.I.C. based design proposal for hot-rolled sections allows for a direct prediction of beams strengths through a formulation describing as accurately as possible the variation in local buckling influence together with the member slenderness. Towards the development of a design formula for welded sections, a local/global coupling function was derived which shall allow for a more precise prediction of the strength of beams made of slender sections, possibly resulting into a shift towards a more extensive use of high strength steel.

Nonetheless, additional investigation is required towards the determination of a leading parameter for welded sections allowing to describe the global response without any significant loss in strength prediction accuracy.

5. Bibliography

Ayrton, W. E., et J. Perry. 1886. «On struts.» *The Engineer* 62.

Beyer, André. 2017. *On the Design of Steel Members with Open Cross-Sections Subject to Combined Axial Force, Bending and Torsion.* PhD thesis, Steel Construction Research Division of CTICM.

Boissonnade, N., et H. Somja. 2012. «Influence of Imperfections in FEM Modeling of Lateral Torsional Buckling.» *Proceedings of the Annual Stability Conference, SSRC.* Grapevine, Texas.

Boissonnade, Nicolas, Marielle Hayeck, Elsy Saloumi, et Joanna Nseir. 2017. «An Overall Interaction Concept for an alternative approach to steel members design.» *Journal of Constructional Steel Research* 135: 199-212.

Couto, Carlos, et Paulo Vila Real. April 2-5, 2019. «On the interaction between local and lateral-torsional buckling of I-shaped slender section beams.» *Proceedings of the Annual Stability Conference, Structural Stability Research Council (SSRC).* St-Louis, Missouri.

Couto, Carlos, Paulo Vila Real, Nuno Lopes, et Bin Zhao. 2016. «Numerical investigation of the lateral-torsional buckling of beams with slender cross sections for the case of fire.» *Engineering Structures* 106: 410-421.

Dux, P. F., et S. Kitipornchai. 1983. «Inelastic Beam Buckling Experiments.» *Journal of Constructional Steel Research* 3 (1): 3-9.

ECCS-Technical Committee 8. 1984. *Publication No. 33: Ultimate Limit State Calculation of Sway Frames with Rigid Joints.*

EN 1993-1-1. 2005. *Eurocode 3: Design of steel structures, Part 1-1 : General rules and rules for buildings.*

EN 1993-1-5. 2005. «Eurocode 3: Design of Steel Structures, Part 1-5: Plated structural elements.»

Gérard, Lucile. 2020. *Contribution to the design of steel I and H-sections members by means of the Overall Interaction Concept.* PhD thesis, Université Laval, Canada.

Gérard, Lucile, Liya Li, Markus Kettler, Donald W. White, et Nicolas Boissonnade. 2020. «Recommendations on the material imperfections definition for the resistance of I-sections.» *Submitted in Thin-Walled Structures.*

Gérard, Lucile, Liya Li, Markus Kettler, et Nicolas Boissonnade. 2019. «Recommendations on the geometrical imperfections definition for the resistance of I-sections.» *Journal of Constructional Steel Research.*

Gérard, Lucile, Liya Li, Markus Kettler, et Nicolas Boissonnade. 2019. «Steel I-sections resistance under compression or bending by the Overall Interaction Concept.» *Submitted in Journal of Constructional Steel Research.*

Hayeck, Marielle. 2016. *Development of a new design method for steel hollow section members resistance.* PhD thesis, PhD thesis, University Of Applied Sciences Of Western Switzerland - Fribourg, University of Liège, Saint-Joseph University Beirut.

Ketter, Robert L. November 1958. «The influence of residual stress on the strength of structural members.» *Welding Research Council Bulletin Series* (44).

Li, Liya, Lucile Gérard, Marielle Hayeck, et Nicolas Boissonnade. 2017. «Stability of Slender Section H.S.S. Columns.» *Proceedings of the Annual Stability Conference, Structural Stability Research Council (SSRC).* San Antonio, Texas.

Liège University, Greisch ingénierie. 2005. *FINELg - NONLINEAR FINITE ELEMENT ANALYSIS PROGRAM - Version 9.0 USER'S MANUAL.* ULG, M&S department; Greisch ingénierie.

Nseir, Joanna. 2015. *Development of a new design method for the cross-section capacity of steel hollow sections.* PhD thesis, University Of Applied Sciences Of Western Switzerland - Fribourg, University of Liège, Saint-Joseph University Beirut.

Prawel, S. P., M. L. Morrell, et G. C. Lee. 1974. «Bending and Buckling Strength of Tapered Structural Members.» *Welding Research Supplement* 75-84.

Schillo, Nicole, et Markus Feldmann. November 7-8 2016. «Interaction of local and global buckling.» *Proceedings of the seventh International Conference on Coupled Instabilities in Metal Structures.* Baltimore, Maryland.

Subramanian, Lakshmi, et Donald W. White. 2017. «Resolving the Disconnects between Lateral Torsional Buckling Experimental Tests, Test Simulations and Design Strength Equations.» *Journal of Constructional Steel Research* 128: 321-334.

Taras, A. 2011. *Contribution to the Development of Consistent Stability Design Rules for Steel Members.* PhD thesis, Institute for steel structures and shell structures, Graz University of Technology, Faculty of Civil Engineering.

Taras, A, et R Greiner. 2010. «New design curves for lateral torsional buckling - Proposal based on a consistent derivation.» *Journal of Constructional Steel Research* 66: 648-663.

Thiébaud, Raphaël. 2014. *Résistance au déversement des poutres métalliques de pont.* Ecole Polytechnique Fédérale de Lausanne, PhD thesis, Ecole Polytechnique Fédérale de Lausanne.

Trahair, N. S. 1993, ISBN 0-8493-7763-3. *Flexural-Torsional Buckling of Structures.* CRC Press.

Villette, Marc. 2003-2004. *Analyse critique du traitement de la barre comprimée et fléchie et propositions de nouvelles formulations.* PhD thesis, Université de Liège, Faculté des Sciences Appliquées.

White, Donald W., et Se-Kwon Jung. November 2004. *Unified Flexural Resistance Equations for Stability Design of Steel I-Section Members – Uniform Bending Tests.* School of Civil and Environmental Engineering, Georgia Institute of Technology, Atlanta: Structural Engineering, Mechanics and Materials, Report No. 04-28, p1-128.

White, Donald W., et Yoon Duk Kim. November 2004. *Unified Flexural Resistance Equations for Stability Design of Steel I-Section Members – Moment Gradient Tests.* School of Civil and Environmental Engineering, Georgia Institute of Technology, Atlanta: Structural Engineering, Mechanics and Materials, Report No. 04-29, p1-149.